Eleventh U.S. National Conference on Earthquake Engineering
Integrating Science, Engineering & Policy
June 25-29, 2018
Los Angeles, California

EXPERIMENTAL STUDY OF CONNECTION BETWEEN FLOOR SYSTEM AND LATERAL FORCE RESISTING SYSTEM

G. Tsampras[1], R. Sause[2], R. Fleischman[3], J. Restrepo[4], Z. Zhang[3], U. Shakya[3], D. Zhang[5], J. Maffei[6], D. Mar[7]

ABSTRACT

This paper presents results from the experimental study of a full-scale deformable connection used to connect the floor system of the gravity load resisting system with the lateral force resisting system (LFRS) of an earthquake-resistant building. Two configurations of the connection are studied. The first configuration consists of a buckling restrained brace (BRB) and steel-reinforced low damping laminated rubber bearings (RB), denoted as BRB+RB. The second configuration of the connection consists of a friction device (FD) and carbon fiber-reinforced low damping laminated rubber bearings (RB), denoted as FD+RB. The connections have stable, repeatable, and well-defined hysteretic nonlinear force-deformation responses that can limit the earthquake-induced horizontal inertial forces transferred from the floor systems to the LFRS. The BRB+RB post-elastic response is mainly controlled by the yielding force of the BRB, the isotropic hardening of the BRB, the dynamic effects on the BRB force-deformation response, and the RB force-deformation response. The FD+RB post-elastic response is controlled by the FD friction force, the effects of the sliding history on the FD friction force, and the RB force-deformation response. The BRB+RB has smaller elastic stiffness than the FD+RB. The steel-reinforced rubber bearings and the carbon fiber-reinforced bearings have approximately linear-elastic force-deformation response. The post-elastic stiffness of the BRB+RB and the FD+RB is mainly determined by the RB stiffness.

[1]Simpson Gumpertz & Heger Inc., Waltham, MA 02453 (email: tsampras.g@gmail.com)
[2]ATLSS Research Center, Dept. of Civil and Environmental Engineering, Lehigh University, Bethlehem, PA 18015
[3]Dept. of Civil Eng. and Eng. Mechanics, University of Arizona, Tucson, AZ 84721
[4]Dept. of Structural Engineering, University of California, San Diego, CA 92037
[5]Dept. of Civil Engineering, Nazarbayev University, Astana, Republic of Kazakhstan 010000
[6]Maffei Structural Engineering, Oakland, CA 94618
[7]Mar Structural Design, Berkeley, CA 94704

Tsampras G., Sause R., Fleischman R., Restrepo J., Zhang Z., Shakya U., Zhang D., Maffei J, Mar D., Experimental study of connection between floor system and lateral force resisting system for the 11NCEE. *Proceedings of the 11th National Conference in Earthquake Engineering*, Earthquake Engineering Research Institute, Los Angeles, CA. 2018.

Eleventh U.S. National Conference on Earthquake Engineering
Integrating Science, Engineering & Policy
June 25-29, 2018
Los Angeles, California

Experimental study of connection between floor system and lateral force resisting system

G. Tsampras[1], R. Sause[2], R. Fleischman[3], J. Restrepo[4], Z. Zhang[3], U. Shakya[3], D. Zhang[5], J. Maffei[6], D. Mar[7]

ABSTRACT

This paper presents results from the experimental study a full-scale deformable connection used to connect the floor system of the gravity load resisting system with the lateral force resisting system (LFRS) of an earthquake-resistant building. Two configurations of the connection are studied. The first configuration consists of a buckling restrained brace (BRB) and steel-reinforced low damping laminated rubber bearings (RB), denoted as BRB+RB. The second configuration of the connection consists of a friction device (FD) and carbon fiber-reinforced low damping laminated rubber bearings (RB), denoted as FD+RB. The connections have stable, repeatable, and well-defined hysteretic nonlinear force-deformation responses that can limit the earthquake-induced horizontal inertial forces transferred from the floor systems to the LFRS. The BRB+RB post-elastic response is mainly controlled by the yielding force of the BRB, the isotropic hardening of the BRB, the dynamic effects on the BRB force-deformation response, and the RB force-deformation response. The FD+RB post-elastic response is controlled by the FD friction force, the effects of the sliding history on the FD friction force, and the RB force-deformation response. The BRB+RB has smaller elastic stiffness than the FD+RB. The steel-reinforced rubber bearings and the carbon fiber-reinforced bearings have approximately linear-elastic force-deformation response. The post-elastic stiffness of the BRB+RB and the FD+RB is mainly determined by the RB stiffness.

Introduction

In a conventional earthquake-resistant building system, the gravity load resisting system (GLRS) includes the floor system, where most of the seismic mass is located, and the floor system is rigidly attached to the lateral force resisting system (LFRS), which resists the earthquake-induced horizontal inertial forces generated by the acceleration of the seismic mass [1] [2]. It has been shown that the seismic inertial forces generated in the floor system can be large relative to the floor

[1]Simpson Gumpertz & Heger Inc., Waltham, MA 02453 (email: tsampras.g@gmail.com)
[2]ATLSS Research Center, Dept. of Civil and Environmental Engineering, Lehigh University, Bethlehem, PA 18015
[3]Dept. of Civil Eng. and Eng. Mechanics, University of Arizona, Tucson, AZ 84721
[4]Dept. of Structural Engineering, University of California, San Diego, CA 92037
[5]Dept. of Civil Engineering, Nazarbayev University, Astana, Republic of Kazakhstan 010000
[6]Maffei Structural Engineering, Oakland, CA 94618
[7]Mar Structural Design, Berkeley, CA 94704

Tsampras G., Sause R., Fleischman R., Restrepo J., Zhang Z., Shakya U., Zhang D., Maffei J, Mar D., Experimental study of connection between floor system and lateral force resisting system for the 11NCEE. *Proceedings of the 11th National Conference in Earthquake Engineering*, Earthquake Engineering Research Institute, Los Angeles, CA. 2018.

diaphragm strength, and can lead to inelastic and potentially non-ductile response of the diaphragm [3]. The development of excessive inertial forces due to high floor accelerations can produce nonlinear response and serious damage of the LFRS, which may lead to unsatisfactory seismic response [4] [5]. The nonlinear response of the LFRS can act as a "cut–off" mechanism that may limit the floor accelerations [6] [7] [8]. However, even when ductile nonlinear response of the LFRS occurs, high floor accelerations may be observed, due to the response contribution of second and higher modes [7] [9]. Studies of LFRS with a predominantly flexural response (e.g. a reinforced concrete cantilever structural wall), which is dominated by nonlinear moment-rotation response at the base of the LFRS, show that high floor accelerations due to the second-mode and higher-mode response can be expected [10] [11] [12] [13] [14] [15]. The kinematic interaction between the LFRS and the floor systems is also expected to increase the overturning moment capacity and the shear force demand in the LFRS [15].

An alternative deformable connection between the floor system of a flexible GLRS and the stiff LFRS of an earthquake-resistant building used to limit the earthquake-induced horizontal inertial forces was presented in [16] [17] [18]. This deformable connection consists of a limited-strength hysteretic component and low-damping laminated rubber bearings. Figure 1 shows a schematic example of a reinforced concrete shear wall earthquake-resistant building with deformable connections. Floor openings are introduced around the LFRS (i.e., shear-walls). The limited-strength hysteretic component transfers the lateral force from the floor system to the LFRS and maintains the stability of the GLRS. The compressive stiffness of the rubber bearings ensures the out-of-plane stability of the LFRS. The shear stiffness of the rubber bearings provides additional post-elastic stiffness to the deformable connection. The vertical motion of the LFRS at each floor level is constrained only by the shear stiffness of the rubber bearings connecting the plane of the LFRS with the floor system.

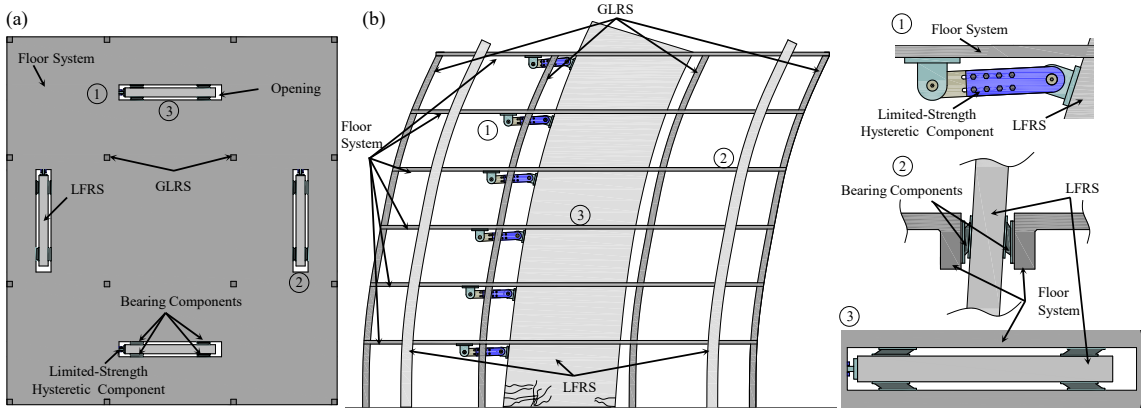


Figure 1: Sketches of an earthquake-resistant building system with deformable connections.

The use of a deformable connection instead of an essentially rigid-elastic (RE) connection at each floor of an example 12-story reinforced concrete shear wall earthquake-resistant building was shown to limit the earthquake-induced horizontal inertial forces transferred from the floor system to the LFRS, and to reduce the floor accelerations [18]. The use of deformable connections with well-defined limited hysteretic force-deformation response significantly reduces the dispersion (due to the variability of the characteristics of the ground motions) in the peak forces transferred from the floor systems to the LFRS, in the peak floor accelerations, and in the peak LFRS story shears [18].

This paper presents a comparison of the experimental force-deformation responses of two full-scale configurations of the deformable connection. The first configuration of the deformable connection consists of a buckling restrained brace (BRB) and steel-reinforced low damping laminated rubber bearings, and it is denoted as BRB+RB [19]. The second configuration of the deformable connection consists of a friction device (FD) and carbon fiber-reinforced low damping laminated rubber bearings, and it is denoted as FD+RB [20].

Experimental set-up

Figure 2 shows the experimental set-up used to test the BRB+RB and the FD+RB connections. A simulated floor system and a reinforced concrete shear wall (i.e., the LFRS) were built in the laboratory. The experimental set-up was designed to test the force-deformation response of the deformable connections subjected to quasi-static and dynamic displacement histories. A detailed description of the test set-up is presented in [19] [20] [21]. Shake table tests [22] [23] [24] show that the deformable connection meets the three dimensional kinematic requirements shown in Figure 1.

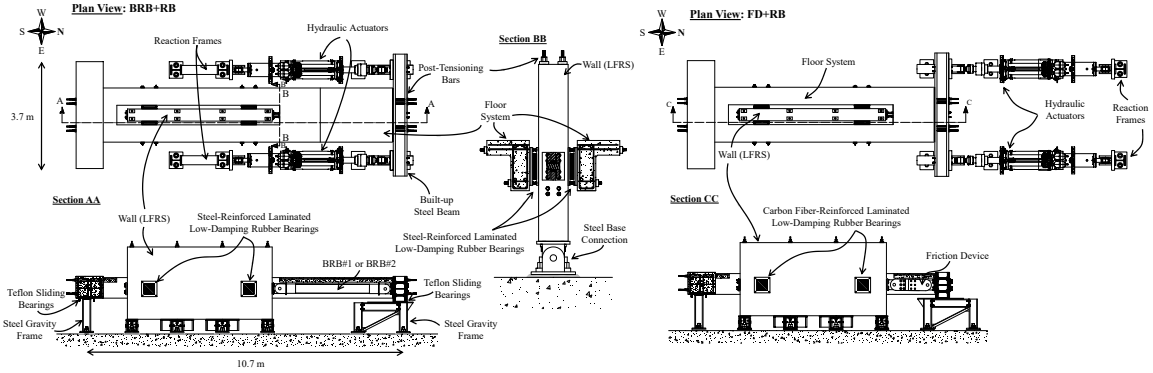


Figure 2: Full-scale test set-up of BRB+RB and FD+RB connections.

Buckling-Restrained Brace

Two BRB+RB connections were tested using two identical BRBs and one set of four steel-reinforced low damping rubber bearings. Figure 3(a) shows the BRB components and Figure 3(b) shows one of the two BRBs installed in the experimental set-up. BRB#1 and BRB#2 had the same nominal dimensions and material properties. Table 1 lists key dimensions of the BRBs. Symbols t, b, and L with the appropriate subscript denote the thickness, width, and length respectively of the yielding zone, transition zone, knife plates, and clevis plates. The yielding zone steel material was ASTM A36 steel [25]. One yielding zone plate was used. L_{yz} was determined from the 2.2% axial strain design limit, assuming the BRB design deformation demand equals 50 mm.

Table 1: BRB component dimensions

Yielding Zone			Transition Zone			Knife Plates			Clevis Plates		
t_{yz} [mm]	b_{yz} [mm]	L_{yz} [m]	t_{tz} [mm]	b_{tz} [mm]	L_{tz} [mm]	t_{kp} [mm]	b_{kp} [mm]	L_{kp} [mm]	t_c [mm]	b_c [mm]	L_c [mm]
25.4	139.2	2.3	25.4	250.4	398.8	38.1	330.2	368.3	63.5	330.2	374.7

The steel modulus of elasticity E_s, the nominal material yielding stress F_{yn}, the actual material yield stress F_{ya} (based on steel coupon test results provided by the BRB manufacturer), the expected nominal

yielding force $P_{by,n}$, the expected actual yielding force $P_{by,a}$, and the material overstrength factor R_y (equal to the ratio of F_{ya} to F_{yn}) are given in Table 2. Figure 3(c) shows the pin load cell used to measure the force in the BRB. Figure 3(d) and (e) show the linear variable displacement transducers (LVDTs) used to measure the axial deformation of the BRB.

Table 2: Material properties and strength of BRB yielding zone

Material	E_s [GPa]	F_{yn} [MPa]	F_{ya} [MPa]	$P_{by,n}$ [kN]	$P_{by,a}$ [kN]	$R_y = F_{ya}/F_{yn}$ [-]
ASTM A36	200	248	282	876	996	1.14

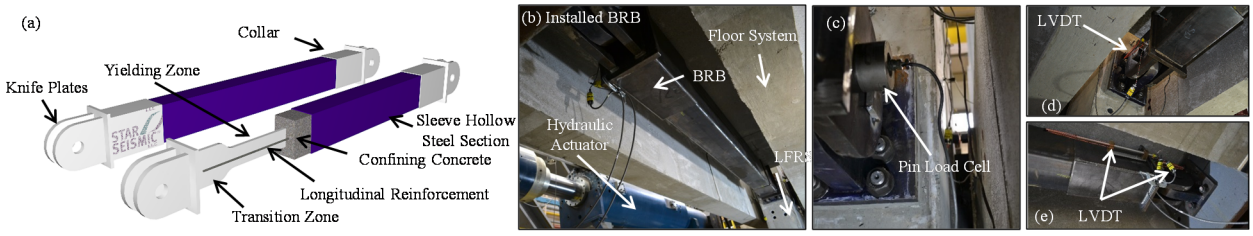


Figure 3: (a) Components of BRB; (b) BRB in test set up; (c), (d), (e) BRB instrumentation.

Friction Device

Figure 4 shows the full-scale FD and its components. Two outer steel plates, one middle steel plate, and two friction shims are clamped using ASTM A325 bolts that are denoted as "friction bolts". The FD has two friction (sliding) interfaces between the middle steel plate and the two friction shims. The friction bolts pass through standard holes [26] in the outer steel plates and the friction shims. These standard holes have 1.6-mm (i.e., 1/16-inch) larger diameter than the diameter of the friction bolts. Slots in the middle steel plate allow the friction bolts, the outer steel plates, and the friction shims to move relative to the middle steel plate (sliding occurs between the friction shims and the inner steel plate). Clevis plates with spherical bearings were used to accommodate the kinematic requirements and to prevent out-of-plane forces (acting normal to the sliding interfaces) from developing in the FD. The FD is symmetric about the longitudinal axis to prevent out-of-plane forces from developing in the FD.

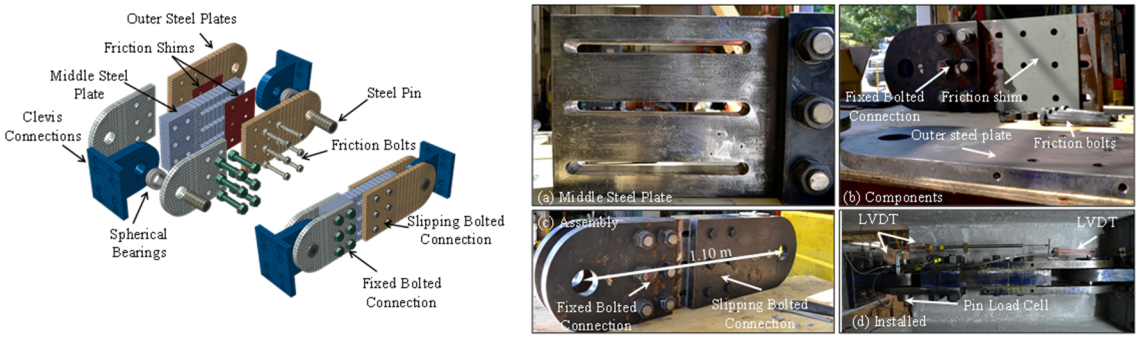


Figure 4: Schematic of full-scale FD components; and (a) Middle steel plate; (b) Other FD components; (c) Assembled FD; (d) Instrumentation of installed FD.

Figure 4(d) shows the pin load cell used to measure the force in the FD and the LVDTs used to measure the axial deformation and sliding of the FD. The FD design deformation is close to 100 mm. The friction force can be estimated using Coulomb theory, $F_s = n_s N \mu_s$, where $n_s = 2$ is the number of friction interfaces, N is the total normal force that the friction bolts apply on the

friction interfaces, and μ_s is the friction coefficient. Six ASTM A325 25.4-mm diameter friction bolts were used. The friction shims were made of the composite material Gatke 398 [27] and the μ_s assumed to be 0.45. The target friction force in the tests discussed in this paper was 735 kN. Additional tests are discussed in [20] [21].

Low-Damping Laminated Rubber Bearings

Two different types of low-damping laminated rubber bearings were tested. One set of four steel-reinforced low-damping laminated rubber bearings was used in the BRB#1+RB and BRB#2+RB connections. One set of four carbon fiber-reinforced low-damping laminated rubber bearings was used in the FD+RB connection. The rubber was 50+/-5 Duro Gr. 3 with estimated shear modulus G = 0.9 MPa, based on the upper bound of G provided by AASHTO [28]. Table 3 lists the dimensions and the expected properties of the each rubber bearing based on the estimated G. W and L are the plan dimensions of the rubber, A is the area of the rubber WL, h_{rt} is the total thickness of the four rubber layers, n_L is the number of rubber layers, S is the shape factor of the rubber layers, K_{RB} is the elastic shear stiffness of the rubber bearing, E_c is the compressive modulus of the rubber bearing, and K_c is the compressive stiffness of the rubber bearing. The expected total shear stiffness of the four rubber bearings is $4K_{RB}$ = 8.8 kN/mm. In the experiments, the total rubber bearings shear force in the four rubber bearings was measured indirectly by subtracting the force measured in the BRB load cell from the sum of the forces in the two actuators.

Table 3: Dimensions and nominal properties of each rubber bearing.

W	L	h_{rt}	n_L	$h_{ri}=h_{rt}/n_L$	$S=A/[2h_{ri}(W+L)]$	G	$K_{RB}=GA/h_{rt}$	$E_c=6GS^2$	$K_c=E_cA/h_{rt}$
[mm]	[mm]	[mm]	[-]	[mm]	[-]	[MPa]	[kN/mm]	[MPa]	[kN/mm]
356	356	50	4	12.5	7.0	0.9	2.2	264	656

Note: Area of the rubber $A=WL$

Experimental Results

Figure 5 shows deformation and force time histories of the BRB+RB and the FD+RB connections due to quasi-static and dynamic sinusoidal displacement histories, and quasi-static earthquake displacement histories. The time has been normalized with respect to the total time of each test. The test number is shown on x-axis.

Test 1 was the first test of BRB#1+RB. Test 10 was the first test of BRB#2+RB. One set of four steel-reinforced rubber bearings was used in Tests 1 through 18. The steel-reinforced rubber bearings had been subjected to limited deformation cycles prior to Test 1.The Gatke398 friction shims were new at the beginning of Test 30. One set of four carbon fiber-reinforced rubber bearings was used in Tests 30 through 45. The carbon fiber-reinforced rubber bearings had been subjected to significant deformation cycles prior to Test 30 while testing other types of friction shims.

The BRB+RB and the FD+RB connections had stable and repeatable hysteretic force-deformation responses under a large number of deformation cycles. The FD+RB post-elastic force-deformation response was controlled by the FD friction force, the effects of the sliding history on the FD friction force, and the RB force-deformation response. The peak FD+RB force under dynamic loading was approximately 15% less than the peak FD+RB force under quasi-static loading. The BRB+RB post-elastic force-deformation response was controlled by the yielding force of the BRB, the isotropic hardening of the BRB, the dynamic effects on the BRB

force-deformation response, and the RB force-deformation response. The dynamic and quasi-static peak BRB+RB forces were similar.

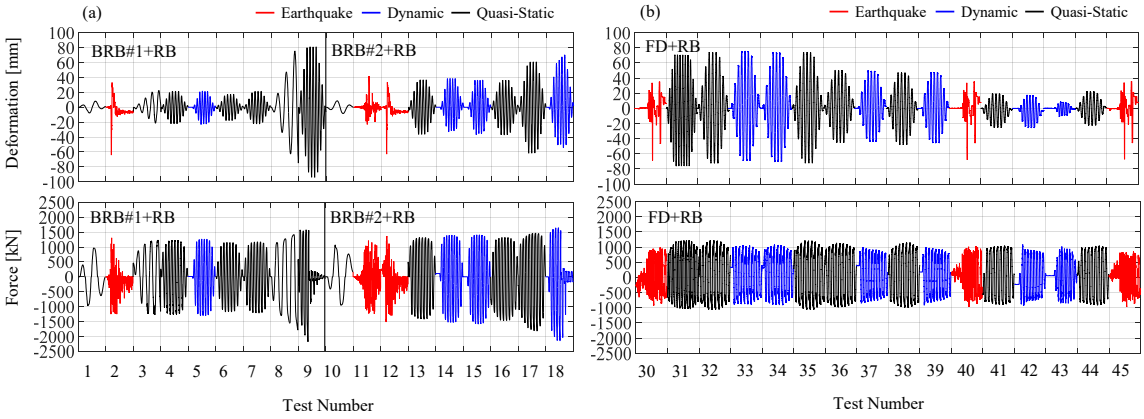


Figure 5: Force and deformation normalized time histories for (a) BRB+RB and (b) FD+RB connections.

Figure 6(a) shows a large amplitude (compared to the 50mm BRB design limit) quasi-static force-deformation response of the FD and the BRBs. The FD elastic stiffness was approximately 1730 kN/mm. The FD had a friction-Coulomb type nonlinear hysteretic force-deformation response. The "break-in" effect, the sliding history, and the dwell time affected the FD friction force [20]. As a result, the FD friction force varied from the target friction force by approximately +/- 15% [20]. The BRB elastic stiffness was approximately 185 kN/mm. Thus, the BRB+RB elastic stiffness was approximately 10 times smaller than the FD+RB elastic stiffness. The BRB had a smooth transition from elastic to post-elastic force-deformation response (i.e., Bauschinger effect). The BRB post-elastic force response is mainly controlled by the BRB isotropic hardening. The BRB isotropic hardening depends on the maximum plastic deformation range experienced by the BRB yielding zone [19]. The BRB kinematic hardening in compression is larger than the BRB kinematic hardening in tension. The difference is mainly due to friction from contact of the yielding zone with the confining concrete when the BRB was in compression and the Poisson's effect [29]. The isotropic and kinematic hardening in the BRB force-deformation response results in significant overstrength that needs to be considered for the design of the clevis connections.

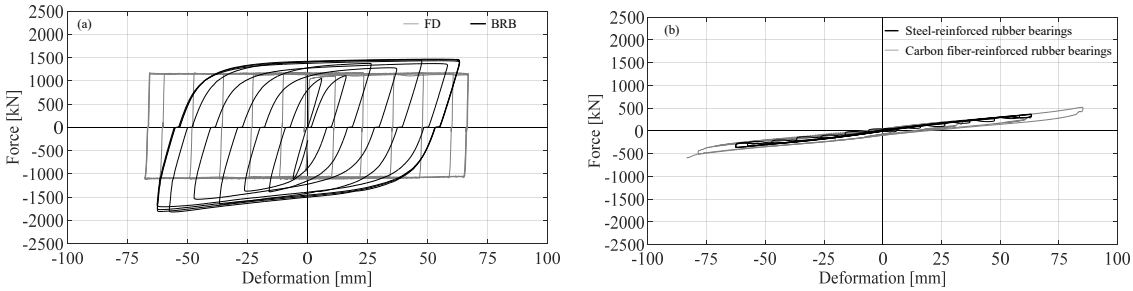


Figure 6: (a) Typical quasi-static force-deformation response of BRB connection and FD connection. (b) Typical shear force-deformation response of steel-reinforced low damping rubber bearings and carbon fiber-reinforced low damping rubber bearings.

Figure 6(b) shows the typical quasi-static force-deformation response of steel-reinforced low-damping laminated rubber bearings from initial tests of BRB#1+RB and carbon fiber-

reinforced low-damping laminated rubber bearings from initial FD+RB tests prior to test 30. Both types of rubber bearings had approximately linear-elastic response with negligible hysteretic behavior compared to the behavior of the FD and the BRB. The effective stiffness of the steel-reinforced rubber bearings and the carbon fiber-reinforced rubber bearings during the first large deformation tests was approximately 6.5 kN/mm.

Figure 7 shows that the quasi-static force-deformation response of the FD+RB connection, the FD, the steel-reinforced rubber bearings, the BRB+RB connection, the BRB, and the carbon fiber-reinforced rubber bearings. The post-elastic stiffness of the FD+RB is determined based on the effective stiffness of the steel-reinforced rubber bearings. The effective stiffness of the carbon fiber-reinforced rubber bearings contributes to the BRB+RB post-elastic stiffness. The post-elastic stiffness of the deformable connections is important to limit their deformation demand.

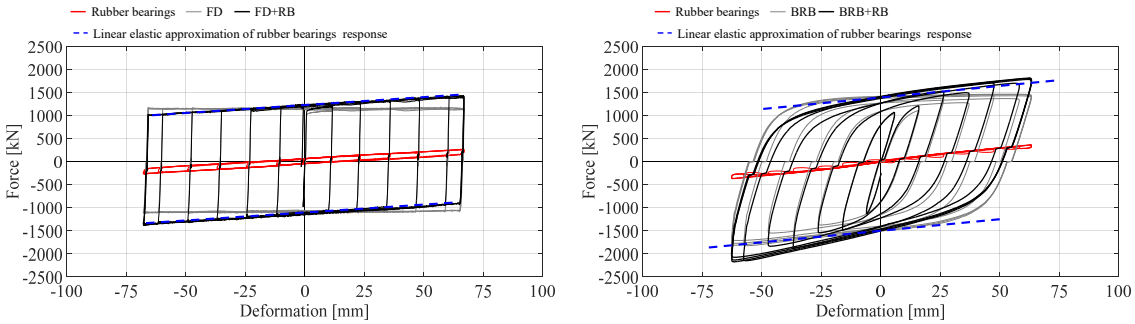


Figure 7: Typical quasi-static force-deformation response of BRB+RB connection, FD+RB connection, and their components.

Figure 8 shows typical quasi-static and dynamic force-deformation responses of the deformable connections. Under dynamic loading the BRB+RB force increased up to 15% compared to the BRB+RB force under quasi-static loading because the BRB force increases as the instantaneous deformation rate increases [19]. The peak BRB+RB force is similar for the quasi-static and dynamic sinusoidal loading because the instantaneous deformation rate is almost zero at peak deformation. Under dynamic loading the FD+RB force decreased up to 15% compared to the FD+RB force under quasi-static loading because the FD force decreases as the maximum (over the displacement history) peak sliding velocity of the FD increases [20].

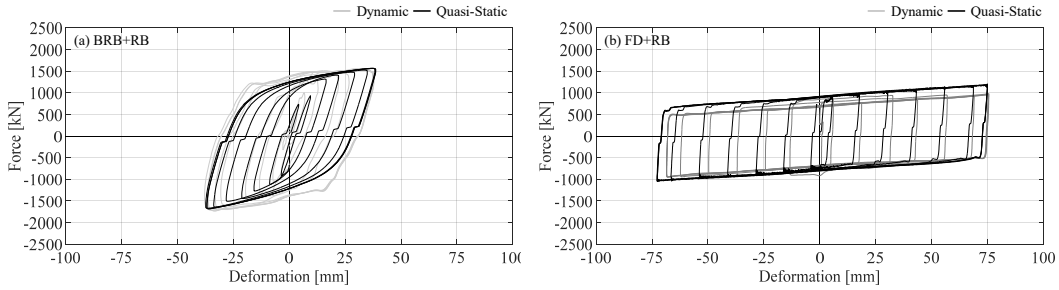


Figure 8: Comparison of typical quasi-static and dynamic force-deformation responses of (a) BRB+RB connection and (b) FD+RB connection.

Conclusions

Experimental results were presented for two configurations of a deformable connection used to connect the floor system of the gravity load resisting system (GLRS) with the lateral load resisting

system (LFRS). The first configuration consisted of a buckling-restrained brace and steel-reinforced low damping rubber bearings (BRB+RB). The second configuration consisted of a friction device and carbon fiber-reinforced low damping rubber bearings (FD+RB).

The deformable connections had stable, repeatable, and well-defined hysteretic nonlinear force-deformation responses that can limit the earthquake-induced horizontal inertial forces transferred from the floor systems to the LFRS. The BRB+RB post-elastic force deformation response is mainly controlled by the yielding force of the BRB, the isotropic hardening of the BRB, the dynamic effects on the BRB force-deformation response, and the RB force-deformation response. The FD+RB post-elastic force deformation response is controlled by the FD friction force, the effects of the sliding history on the FD friction force, and the RB force deformation response. The BRB+RB had 10 times smaller elastic stiffness than the FD+RB. The steel-reinforced rubber bearings and the carbon fiber-reinforced bearings have approximately linear-elastic force deformation response. The post-elastic stiffness of the BRB+RB and the FD+RB is mainly determined by the RB stiffness.

Acknowledgments

This paper is based upon work supported by grants from National Science Foundation, Award No. CMMI-1135033 in the George E. Brown, Jr. Network for Earthquake Engineering Simulation Research (NEESR) program, and Award No. CMMI-0402490 for the George E. Brown, Jr. Network for Earthquake Engineering Simulation (NEES) consortium operations. The authors are grateful for additional financial support provided by the Gerondelis Foundation, Yen Fellowship, and Lehigh University. The contributions Dr. Shivaglal Cheruvalath, and the NEES@Lehigh and ATLSS Center staff are acknowledged. The authors appreciate the contribution of the companies DYMAT™, Star Seismic®, and Scan-Pac Mfg, Inc. Any opinions, findings, and conclusions expressed in this report are those of the authors and do not necessarily reflect the views of the National Science Foundation or others acknowledged here.

References

1 J. P. Moehle, J. D. Hooper, D. J. Kelly and T. R. Meyer "Seismic design of cast-in-place concrete diaphragms, chords, and collectors," National Institute of Standards and Technology, 2010.

2. R. Sabelli, T. A. Sabol and S. W. Easterling, "Seismic design of composite steel deck and concrete-filled diaphragms," National Institute of Standards and Technology, 2011.
3. R. Fleischman and K. Farrow, "Dynamic behavior of perimeter lateral-system structures with flexible diaphragms," *Earthquake Engineering and Structural Dynamics,* vol. 30, no. 5, pp. 745-763, 2001.
4. M. Rodriguez, J. Restrepo and A. Carr, "Earthquake - induced floor horizontal accelerations in buildings," *Earthquake Engineering and Structural Dynamics,* pp. 693-718, 2002.
5. M. Rodriguez, J. Restrepo and J. Blandon, "Seismic design forces for rigid floor diaphragms in precast concrete building structures," *Journal of Structural Engineering,* pp. 1604-1615, 2007.
6. T. Kelly, "Floor response of yielding structures," *Bulletin of New Zealand National Society for Earthquake Engineering,* pp. 255-272, 1978.
7. S. Ray-Chaudhuri and T. Hutchinson, "Effect of nonlinearity of frame buildings on peak horizontal floor acceleration," *Journal of Earthquake Engineering,* pp. 124-142, 2011.
8. F. X. Flores, D. Lopez-Garcia and F. A. Charney, "Assessment of floor accelerations in special steel moment frames," *Journal of Constructional Steel Research,* vol. 106, pp. 154-165, 2015.
9. R. Sewell, A. Cornell, G. Toro and R. McGuire, "A study of factors influencing floor response spectra in

nonlinear multi-degree-of-freedom structures," The John A. Blume Earthquake Engineering Center Report No. 82, 1986.

10. A. K. Chopra, Dynamics of Structures, Berkeley,CA, California: Pearson Prentice Hall, 2007.
11. D. Roke, "Damage-free seismic-resistant self-centering concentrically-braced frames," Ph.D. Dissertation, Lehigh University, Bethlehem,PA, 2010.
12. A. D. Amaris Mesa, "Dynamic amplification of seismic moments and shear forces in cantilever walls," M.Sc. Thesis, University of Pavia, Pavia, 2002.
13. L. Wiebe and C. Christopoulos, "Mitigation of higher mode effects in base-rocking systems by using multiple rocking sections," *Journal of Earthquake Engineering,* pp. 83-108, 2009.
14. L. Wiebe, C. Christopoulos, R. Trembley and M. Leclere, "Mechanisms to limit higher mode effects in a controlled rocking steel frame. 1: Concept, modelling, and low-amplitude shake table testing," *Earthquake Engineering and Structural Dynamics,* pp. 1053-1068, 2013.
15. M. Panagiotou, J. I. Restrepo and J. P. Conte, "Shake-table test of a full-scale 7-story building slice. Phase I: Rectangular wall," *Journal of Structural Engineering,* vol. 137, no. 6, pp. 691-704, 2011.
16. D. Zhang, R. Fleischman and Z. Zhang, "Analytical Investigation of Seismic Behavior of Building Structures with an Inertial Force-Limiting Floor Anchorage System," *International Journal of Engineering and Technology,,* vol. 8, no. 4, pp. 234-240, 2016.
17. R. Fleischman, J. Restrepo, A. Nema, D. Zhang, U. Shakya, Z. Zhang, R. Sause, G. Tsampras and G. Monti, "Inertial Force-Limiting Anchorage System for Seismic Resistant Building Structures," in *Structures Congress 2015*, Portland, OR, 2015.
18. G. Tsampras, R. Sause, D. Zhang, R. B. Fleischman, J. I. Restrepo, D. Mar and J. Maffei, "Development of deformable connection for earthquake-resistant buildings to reduce floor accelerations and force responses," *Earthquake Engineering and Structural Dynamics,* vol. 45, no. 9, p. 1473–1494, 2016.
19. G. Tsampras, R. Sause, R. Fleischman and J. Restrepo, "Experimental study of deformable connection consisting of buckling-restrained brace and rubber bearings to connect floor system to lateral force resisting system," *Earthquake Engineering & Structural Dynamics,* vol. 46, no. 8, pp. 1287-1305, 2016.
20. G. Tsampras, R. Sause, R. Fleischman and J. Restrepo, "Experimental study of deformable connection consisting of friction device and rubber bearings to connect floor system to lateral force resisting system," *Earthquake Engineering & Structural Dynamics,* 2017, DOI: 10.1002/eqe.3004.
21. G. Tsampras and R. Sause, "Development and experimental validation of deformable connection for earthquake-resistant building systems with reduced floor accelerations," Network of Earthquake Engineering Simulation (NEES) Technical Report, https://nees.org/resources/13612, 2015.
22. D. Zhang, R. Fleischman, J. Restrepo, R. Sause, J. Maffei, D. Mar and G. Monti, "Development of a Floor Inertia Force Limiting Anchorage System under Earthquake Loading," in *10th U.S. National Conference on Earthquake Engineering (10NCEE) / NEES Quake Summit*, Anchorage, AK, 2014.
23. R. Fleischman, J. Restrepo, A. Nema, D. Zhang, U. Shakya, Z. Zhang, R. Sause, G. Tsampras and G. Monti, "Inertial Force-Limiting Anchorage System for Seismic Resistant Building Structures," in *2015 Structures Congress*, Portland, OR, 2015.
24. Z. Zhang, R. Fleischman, J. Restrepo, G. Guerrini, A. Nema, D. Zhang, U. Shakya, G. Tsampras and R. Sause, "Shake table test performance of an inertial force-limiting floor anchorage system," *Earthquake Engineering & Structural Dynamics.*
25. ASTM A36/A36M - 14, "Standard specification for carbon structural steel," American Society for Testing and Materials, 2014.
26. AISC, Steel Construction Manual, Americal Institute of Steel Construction, 2010.
27. Scan Pan Inc., "Gatke Material Selection Guide," Menomonee Falls, WI, USA, 2010.
28. AASHTO, LRFD Bridge Design Specification, Washington, DC, 2010.
29. B. Saxey and M. Daniels, "Characterization of overstrength factors for buckling restrained braces," in *Proceedings in Australian Structural Engineering Conference 2014*, Auckland, NZ, 2014.